

# 6

## Corrections to nonlinear evolution equations

In this chapter we describe developments at the very forefront of research on nonlinear evolution equations. We first outline the calculation of running-coupling corrections to the BFKL, BK, and JIMWLK evolution equations. Such corrections slow down the growth of the saturation scale with energy, putting the predictions of saturation physics more in line with the experimental data. We then discuss the next-to-leading order (NLO) corrections to the BFKL and BK evolutions, which resum the subleading logarithms of energy, i.e., powers of  $\alpha_s^2 Y$ . The NLO BFKL corrections are rather large numerically; we present a proposal for resumming these large corrections to all orders that results in a reduction in their net effect on the LO calculation. Owing to the highly technical nature of many of the results presented, in most topics considered in this chapter we will merely outline the main points of the derivation. Interested readers can find the calculational details in the references supplied.

### 6.1 Why we need higher-order corrections

There are several reasons to study higher-order corrections to the BFKL, BK, and JIMWLK evolution equations presented in the previous chapters. Some reasons are theoretical, some are phenomenological, and some are both.

On the phenomenological side, the LO BFKL approach encounters a very simple problem. The BFKL pomeron intercept given by Eq. (3.86) is

$$\alpha_P - 1 \approx 2.77\bar{\alpha}_s, \quad (6.1)$$

which, for a phenomenologically reasonable value of the strong coupling  $\alpha_s$ , say 0.3, gives  $\alpha_P - 1 \approx 0.79$ , which is too large to describe any existing data in DIS, proton–proton, or nuclear collisions. One would therefore hope that higher-order corrections would lower this result, pushing the theory closer to the data.

On the more theoretical side we note that the BFKL, BK, and JIMWLK equations were derived in earlier chapters for fixed coupling constant. A question arises concerning the value of the coupling constant that should be used; this is important, since the validity of the whole saturation approach depends on whether the coupling is small. Theoretically we cannot answer this question from fixed-coupling calculations; one has to perform higher-order calculations to fix the scale of the running-coupling constant. This question about the

scale of the coupling also has phenomenological importance, since one has to know which values of the coupling to use in comparing the small- $x$  evolution with experiment.

The BK equation derived earlier contains powers of  $\alpha_s N_c Y$  resummed through large- $N_c$  LLA evolution along with powers of  $\alpha_s^2 A^{1/3}$  resummed by the GGM initial conditions. Generalizing BK to JIMWLK relaxes the large- $N_c$  approximation: the JIMWLK equation resums powers of  $\alpha_s Y$  and  $\alpha_s^2 A^{1/3}$ . Both the LO BK and LO JIMWLK evolutions are valid as long as the NLO corrections are small, i.e., for  $\alpha_s^2 Y \ll 1$ , which means  $Y \ll 1/\alpha_s^2$ . Therefore, the problem of calculating the NLO correction to the BFKL, BK, and JIMWLK kernels is very important for understanding the region of applicability of the high density QCD theory in the form that has been developed above and for further extension of this region. Corrections to the initial conditions for the evolution equations (for instance, terms containing powers of  $\alpha_s^4 A^{1/3}$ ) are also important, both theoretically and phenomenologically; however, attempts to calculate those have not reached the level required for coherent presentation in a book and will not be described here.

From a purely theoretical standpoint it is also important to understand whether the expansion in logarithms of  $1/x$  is stable, that is, whether one can calculate corrections to the LO result and whether such corrections are finite (after all the standard field-theoretical divergences have been taken into consideration). Again, this question is, in the end, related to the first, purely phenomenological, one: what are the size and the sign of the NLO corrections?

The presentation below attempts to answer many of the above questions.

## 6.2 Running-coupling corrections to the BFKL, BK, and JIMWLK evolutions

We begin by calculating the scale of the running-coupling constant in the BFKL, BK, and JIMWLK evolution equations. The running-coupling corrections to small- $x$  evolution are calculated following the Brodsky–Lepage–Mackenzie (BLM) scale-setting procedure (Brodsky, Lepage, and Mackenzie 1983). Working in the setting we used for the derivation of the JIMWLK and BK evolutions, below we will first resum the contributions of all quark-loop corrections to the LLA kernel. Each quark-loop correction brings in a power of  $\alpha_\mu N_f$ , with  $N_f$  the number of quark flavors (see Sec. 1.5) and  $\alpha_\mu = \alpha_s(\mu^2)$  the physical coupling at some arbitrary renormalization scale  $\mu$ . Inspired by Abelian gauge theories, Brodsky, Lepage, and Mackenzie (1983) argued that the powers of  $\alpha_\mu N_f$  come mainly from the powers of the one-loop QCD beta function, that is, from the powers of  $\alpha_\mu \beta_2$ , where  $\beta_2$  is given in Eq. (1.89). Following the BLM prescription, we will then complete  $N_f$  to the full coefficient of the one-loop beta function by means of the replacement

$$N_f \rightarrow -6\pi\beta_2 \quad (6.2)$$

in the expression obtained by including quark-loop corrections in the BK and JIMWLK kernels. After this, the powers of  $\alpha_\mu \beta_2$  should combine to give the physical running coupling  $\alpha_s(Q^2)$  defined in Eq. (1.88) at the various momentum scales  $Q$  that would follow from this calculation.

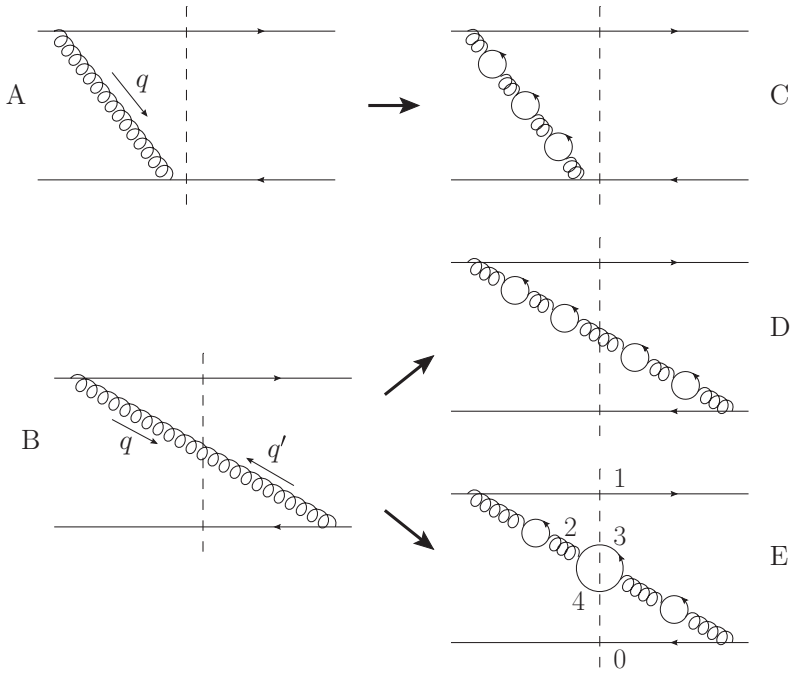


Fig. 6.1. Diagrams with quark-loop corrections to the BK and JIMWLK evolution kernels. The iteration of quark-loop insertions to all orders is implied in each graph on the right.

The original BLM prescription did not address the diagrams with gluon–gluon interactions. Here we will assume that the prescription is still valid for diagrams with triple-gluon vertices. This statement has not been rigorously proven, though in small- $x$  physics it was explicitly verified in the NLO BK calculation by Balitsky and Chirilli (2008). A complementary way of thinking about a running-coupling calculation is by defining it as a resummation of  $\alpha_s N_f$ -corrections to the LO BFKL, BK, and JIMWLK kernels, the completion of  $N_f$  to the full beta function using (6.2) being an intelligent guess at the size of the gluon contribution, explicitly confirmed at NLO.

### 6.2.1 An outline of the running-coupling calculation

The main types of diagrams containing quark-loop corrections to the LO BK and JIMWLK evolution kernels are shown in Fig. 6.1 using the notation of Figs. 5.8, 5.9, and 5.10. The vertical dashed line again denotes the interaction with the target (or the subsequent evolution along with the interaction with the target). On the left of Fig. 6.1 we show one virtual (A) and one real (B) diagram contributing to one step of the LO BK or JIMWLK evolutions (cf. Fig. 5.9). All other real and virtual diagrams in the evolution kernel generated by connecting the gluon line to the quark and antiquark lines in all possible ways (see Figs. 5.9 and 5.10)

should be included in the calculation; they are not shown explicitly. For LCPT diagrams, instantaneous terms like those shown in Fig. 4.14 need to be included as well.

The running-coupling corrections for the BK and JIMWLK kernels are obtained by inserting all-order quark bubbles into the gluon propagator in all possible ways. On the right of Fig. 6.1 we show the quark-loop-corrected diagrams corresponding to the fixed-coupling graphs on the left. The virtual correction (in the upper-left panel, labeled A) gives rise only to one class of diagrams, with quark loops iterated on the gluon propagator to all orders, shown in panel C. Working in momentum space, it is clear that the quark bubbles in this case form a geometric series, which is resummed to give

$$\alpha_s(q_\perp^2) = \frac{\alpha_\mu}{1 + \alpha_\mu \beta_2 \ln(q_\perp^2/\mu^2)}, \tag{6.3}$$

where we have used the replacement (6.2) to complete  $N_f$  to the full beta function, and the factor  $\alpha_\mu$  in the numerator comes from the coupling of the gluon to the parent dipole. We see how physical running coupling emerges for the virtual diagrams. The coupling runs with the transverse momentum of the gluon line  $q_\perp$ ; this can be found by calculating the diagram in panel C of Fig. 6.1 in, say, LCPT (Kovchegov and Weigert 2007a).

The real-emission diagram B generates two classes of quark-loop corrections, as shown in the lower two panels on the right of Fig. 6.1, labeled D and E. The first class of corrections, shown in panel D, corresponds to the case when it is the gluon that interacts with the target. This is to be compared to the other class of corrections, where the gluon fluctuates into a  $q\bar{q}$  pair, which is still in the wave function at the time it enters the nucleus, so that now the quark and antiquark in the pair interact with the nucleons, as depicted in panel E of Fig. 6.1.

The momenta of the gluon line to the left and to the right of the interaction with the target are different in general: we label them  $q$  and  $q'$  respectively, as shown in panel B of Fig. 6.1. Note that the running-coupling corrections to the interaction of the gluon (and now  $q\bar{q}$ ) cascade with the target factorize from the running-coupling corrections to the small- $x$  evolution and are included separately (Balitsky 2007, Kovchegov and Weigert 2007b). Concentrating on the evolution, we see that the quark bubbles in the diagrams like that in panel D of Fig. 6.1 give us two separate geometric series, one to the left and one to the right of the interaction with the target. We thus get

$$\frac{\alpha_\mu}{[1 + \alpha_\mu \beta_2 \ln(q_\perp^2/\mu^2)] [1 + \alpha_\mu \beta_2 \ln(q'^2_\perp/\mu^2)]} = \frac{\alpha_s(q_\perp^2) \alpha_s(q'^2_\perp)}{\alpha_\mu}, \tag{6.4}$$

where again we have used Eq. (6.2) to complete  $N_f$  to the full beta function and the factor  $\alpha_\mu$  stems from the coupling of the gluon to the dipole. We can see a problem with Eq. (6.4): using Eq. (1.88) we cannot rewrite it as a product of powers of the running coupling only, as we did in Eq. (6.3). One factor  $\alpha_\mu$  would still remain, as shown on the right of Eq. (6.4). Hence diagrams in the class represented by panel D cannot be expressed in terms of the running couplings only.

To resolve the issue we have to include the diagram in panel E as well. At first glance, the diagrams in this class, just as in the panel D class, would seem to have two geometric

series but now with a factor of  $\alpha_\mu^2$  in the numerator; the extra coupling arises from the coupling of gluons to the quark bubble that interacts with the target (which is slightly larger than the other bubbles in panel E). This would give

$$\frac{\alpha_\mu^2}{[1 + \alpha_\mu \beta_2 \ln(q_\perp^2/\mu^2)] [1 + \alpha_\mu \beta_2 \ln(q'_\perp{}^2/\mu^2)]} = \alpha_s(q_\perp^2) \alpha_s(q'_\perp{}^2). \tag{6.5}$$

However, this cannot be the complete answer. For one thing, it seems absurd that one power of the fixed coupling, corresponding to the gluon emission and absorption, has been replaced by two powers of the running coupling, making the evolution kernel contribution of order  $\alpha_s^2$ . Analyzing the matter further, one realizes that the quark loop that interacts with the target also brings in a factor  $N_f$  that should be completed to  $\beta_2$  and, more importantly, that the integration over momentum in the loop leads to a UV divergence, i.e., generates a  $\ln \mu^2$  term. Keeping this logarithmically divergent term, we write the contribution of diagram E in Fig. 6.1 to the running of the coupling as

$$\frac{\alpha_\mu^2 \beta_2 \ln(Q^2/\mu^2)}{[1 + \alpha_\mu \beta_2 \ln(q_\perp^2/\mu^2)] [1 + \alpha_\mu \beta_2 \ln(q'_\perp{}^2/\mu^2)]}; \tag{6.6}$$

the scale  $Q$  is determined by an explicit calculation. Adding Eqs. (6.4) and (6.6) we see that diagrams D and E combine to give

$$\frac{\alpha_\mu [1 + \alpha_\mu \beta_2 \ln(Q^2/\mu^2)]}{[1 + \alpha_\mu \beta_2 \ln(q_\perp^2/\mu^2)] [1 + \alpha_\mu \beta_2 \ln(q'_\perp{}^2/\mu^2)]} = \frac{\alpha_s(q_\perp^2) \alpha_s(q'_\perp{}^2)}{\alpha_s(Q^2)}. \tag{6.7}$$

We see that now the answer for the real graphs is expressible in term of factors of the running coupling only. Note the unexpected structure of the result (6.7): in the BK and JIMWLK evolution kernels, one factor of the fixed coupling  $\alpha_s$  in the LO evolution kernel is replaced by three running couplings, two in the numerator and one in the denominator,

$$\alpha_\mu \longrightarrow \frac{\alpha_s(q_\perp^2) \alpha_s(q'_\perp{}^2)}{\alpha_s(Q^2)}, \tag{6.8}$$

so that the answer is still order  $\alpha_s$ . This structure is sometimes referred to as a *triumvirate* of couplings. It was first postulated for the running-coupling corrections to the BFKL evolution by Braun (1995) and Levin (1995). It was explicitly derived for the BFKL, BK, and JIMWLK evolution equations by Balitsky (2007) and by Kovchegov and Weigert (2007a).

The detailed calculation of the scale  $Q$  with explicit demonstrations that  $q_\perp$  and  $q'_\perp$  set the scales for the other two couplings in (6.7), along with the Fourier transform of the answer into transverse coordinate space, are too technically involved to be presented here in any detail. We refer the interested reader to the papers Balitsky (2007), Kovchegov and Weigert (2007a, b), and Gardi *et al.* (2007). We simply quote here the final answer for the running-coupling BK equation.

Writing the BK evolution equation (4.137) as

$$\partial_Y S(\vec{x}_{1\perp}, \vec{x}_{0\perp}, Y) = \int d^2x_2 K(\vec{x}_{1\perp}, \vec{x}_{0\perp}, \vec{x}_{2\perp}) \times [S(\vec{x}_{1\perp}, \vec{x}_{2\perp}, Y) S(\vec{x}_{2\perp}, \vec{x}_{0\perp}, Y) - S(\vec{x}_{1\perp}, \vec{x}_{0\perp}, Y)], \tag{6.9}$$

we note that the LO dipole kernel is

$$K_{LO}(\vec{x}_{1\perp}, \vec{x}_{0\perp}, \vec{x}_{2\perp}) = \frac{\alpha_s N_c}{2\pi^2} \frac{x_{10}^2}{x_{20}^2 x_{21}^2}. \tag{6.10}$$

The form of the running-coupling kernel depends on how one extracts the scale  $Q$  shown in Eqs. (6.6)–(6.8); while  $\ln \mu^2$  in  $\ln(Q^2/\mu^2)$  is identified unambiguously, it is less clear how to define uniquely the scale  $Q^2$ . The problem originates in the fact that the contribution to the evolution kernel coming from diagram E in Fig. 6.1 cannot even be cast into the form (6.9). In the large- $N_c$  limit this diagram has two dipoles interacting with the target: the dipole 13, consisting of the original quark and antiquark of the  $q\bar{q}$  pair fluctuation of the gluon, and the dipole 40, consisting of the quark in the pair and the antiquark in the parent dipole (the coordinates are defined in Fig. 6.1E). The two dipoles do not have a common transverse coordinate, therefore their contribution is not of the form (6.9) and actually includes integrals over both  $\vec{x}_{3\perp}$  and  $\vec{x}_{4\perp}$ , with the kernel dependent on four points in the transverse plane,  $\vec{x}_{1\perp}, \vec{x}_{0\perp}, \vec{x}_{3\perp}, \vec{x}_{4\perp}$ . The UV divergence that we need stems from the region between  $\vec{x}_{3\perp}$  and  $\vec{x}_{4\perp}$ , and can be extracted either by integrating over  $\vec{x}_{3\perp}$  while keeping  $\vec{x}_{4\perp}$  fixed (the Balitsky (2007) prescription) or by integrating over  $\vec{x}_{3\perp}$  and  $\vec{x}_{4\perp}$  keeping the gluon position  $\vec{x}_{2\perp}$  (see Fig. 6.1E) fixed (the Kovchegov and Weigert (2007a) prescription). The gluon position is related to  $\vec{x}_{3\perp}$  and  $\vec{x}_{4\perp}$  via the following expression (cf. Eq. (1.87) along with the discussion after it, as well as Fig. 1.4):

$$\vec{x}_{2\perp} = z_3 \vec{x}_{3\perp} + (1 - z_3) \vec{x}_{4\perp} \tag{6.11}$$

with  $z_3$  the fraction of the gluon’s light cone momentum carried by quark 3. (Indeed, other extractions of the UV divergence are also possible but calculations have been done only for the two cases mentioned.)

The kernel of the running-coupling BK evolution (rcBK) in the Balitsky prescription is (Balitsky 2007)

$$K_{rc}^{Bal}(\vec{x}_{1\perp}, \vec{x}_{0\perp}, \vec{x}_{2\perp}) = \frac{N_c \alpha_s(x_{10}^2)}{2\pi^2} \left[ \frac{x_{10}^2}{x_{20}^2 x_{21}^2} + \frac{1}{x_{20}^2} \left( \frac{\alpha_s(x_{20}^2)}{\alpha_s(x_{21}^2)} - 1 \right) + \frac{1}{x_{21}^2} \left( \frac{\alpha_s(x_{21}^2)}{\alpha_s(x_{20}^2)} - 1 \right) \right], \tag{6.12}$$

where we have used the abbreviated notation

$$\alpha_s(x_{\perp}^2) = \alpha_s \left( \frac{4e^{-5/3-2\gamma_E}}{x_{\perp}^2} \right) \tag{6.13}$$

and the coupling on the right is defined by Eq. (1.88) in the  $\overline{\text{MS}}$  renormalization scheme.

In the Kovchegov–Weigert prescription the rcBK kernel is (Kovchegov and Weigert 2007a)

$$\begin{aligned}
 &K_{rc}^{KW}(\vec{x}_{1\perp}, \vec{x}_{0\perp}, \vec{x}_{2\perp}) \\
 &= \frac{N_c}{2\pi^2} \left[ \alpha_s(x_{20}^2) \frac{1}{x_{20}^2} - 2 \frac{\alpha_s(x_{20}^2)\alpha_s(x_{21}^2)}{\alpha_s(R^2)} \frac{\vec{x}_{20} \cdot \vec{x}_{21}}{x_{20}^2 x_{21}^2} + \alpha_s(x_{21}^2) \frac{1}{x_{21}^2} \right], \tag{6.14}
 \end{aligned}$$

with the scale  $R^2$  given by

$$R^2 = x_{20} x_{21} \left( \frac{x_{21}}{x_{20}} \right)^\Xi, \tag{6.15}$$

where

$$\Xi = \frac{x_{20}^2 + x_{21}^2}{x_{20}^2 - x_{21}^2} - 2 \frac{x_{20}^2 x_{21}^2}{\vec{x}_{20} \cdot \vec{x}_{21}} \frac{1}{x_{20}^2 - x_{21}^2}.$$

The two prescriptions (6.12) and (6.15) neglect different contributions of the diagram in Fig. 6.1E; as was shown by Albacete and Kovchegov (2007b), when the neglected terms are put back in, the two calculations agree with each other. It was also shown by an explicit numerical evaluation that the Balitsky prescription, when used in the BK evolution, gives a result that is closer to the full answer obtained by using the full diagram in Fig. 6.1E in the kernel of the small- $x$  evolution (Albacete and Kovchegov 2007b). This is probably related to the fact that in the Balitsky prescription one obtains the linear (BFKL) part of the equation exactly: it gives the contribution correctly when only one dipole in Fig. 6.1E (either 13 or 40) interacts with the target. In Sec. 4.5.1 we saw that a good approximation to the solution of the fixed-coupling BK equation can be constructed by solving the linear BFKL equation with a saturation boundary in the IR (Gribov, Levin, and Ryskin 1983, Mueller and Triantafyllopoulos 2002). Most probably the same is true in the running-coupling case (see Gribov, Levin, and Ryskin (1983), Section 2.3.2), justifying the fact that the Balitsky prescription gives the full answer more accurately.

The evolution kernel of the running-coupling JIMWLK (rcJIMWLK) equation has been calculated only using the Kovchegov–Weigert prescription and can be found in Kovchegov and Weigert (2007a).

Once one has the running-coupling corrections to the nonlinear evolution equations, it is possible to obtain the running-coupling version of the BFKL equation. We first define the unintegrated gluon distribution  $\phi(k_\perp, Y)$ , using the dipole amplitude  $N$ , by (cf. Eqs. (3.92), (4.98))

$$\int d^2b N(\vec{x}_\perp, \vec{b}_\perp, Y) = \frac{2\pi}{N_c} \int d^2k_\perp \left( 1 - e^{i\vec{k}_\perp \cdot \vec{x}_\perp} \right) \frac{\alpha_s(k_\perp^2)}{k_\perp^2} \phi(k_\perp, Y) \tag{6.16}$$

(Levin and Ryskin 1987). This connection between  $\phi$  and  $N$  follows from the two-gluon exchange depicted in Fig. 6.2 (in the notation of Fig. 4.3), and, while its validity in the nonlinear saturation regime may be questioned, it is valid in the linear regime in which we want to apply it.

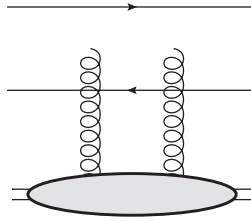


Fig. 6.2. The lowest-order diagram contributing to the relation between the dipole amplitude  $N$  and the unintegrated gluon distribution  $\phi$ .

Using Eq. (6.16) in Eq. (6.9) with the kernel given by Balitsky prescription Eq. (6.12) (for which, in momentum space,  $Q^2 = k_{\perp}^2$ ), linearizing the result, and Fourier-transforming it into momentum space, one obtains the running-coupling BFKL (rcBFKL) equation for the unintegrated gluon distribution (Kovchegov and Weigert 2007b):

$$\begin{aligned} \partial_Y \phi(k_{\perp}, Y) = & \frac{N_c}{\pi^2} \int \frac{d^2 q}{(\vec{k}_{\perp} - \vec{q}_{\perp})^2} \\ & \times \left[ \alpha_s \left( (\vec{k}_{\perp} - \vec{q}_{\perp})^2 \right) \phi(q_{\perp}, Y) - \frac{k_{\perp}^2}{2q_{\perp}^2} \frac{\alpha_s(q_{\perp}^2) \alpha_s \left( (\vec{k}_{\perp} - \vec{q}_{\perp})^2 \right)}{\alpha_s(k_{\perp}^2)} \phi(k_{\perp}, Y) \right]. \end{aligned} \tag{6.17}$$

This equation was originally conjectured by Braun (1995) and Levin (1995) by requiring that the bootstrap property of BFKL is preserved after running-coupling corrections are included. Equation (6.17) can be compared with the fixed-coupling BFKL evolution of Eq. (3.94). One sees that, for the real term (the first term on the right-hand side of Eq. (6.17)), the coupling constant runs with the momentum in the rung (the  $s$ -channel gluon) of the BFKL ladder while in the virtual term (the second term on the right) a triumvirate structure arises for the three momenta involved in the color-octet gluon reggeization diagrams (see e.g. Fig. 3.11).

### 6.2.2 Impact of running coupling on small- $x$ evolution

The effects of the running-coupling corrections on the small- $x$  evolution can be summarized as follows.

- (i) They slow down the evolution, by reducing the growth rates of the amplitude  $N(x_{\perp}, Y)$  and of the saturation scale  $Q_s(Y)$  with energy or rapidity.
- (ii) They preserve geometric scaling in the vicinity of the saturation scale ( $x_{\perp} \sim 1/Q_s(Y)$ ) while changing the profile of the dipole amplitude  $N(x_{\perp}, Y)$  as a function of  $x_{\perp} Q_s(Y)$ .
- (iii) They make the saturation scale  $Q_s$  independent of the atomic number  $A$  at very small  $x$ , thus eliminating the nuclear enhancement that we saw in the GGM model (Eq. (4.52)) and in the fixed-coupling small- $x$  evolution (Eq. (4.156)).

These properties can be derived from a numerical solution of the rcBK equation or by analytical methods. The numerical solution of the rcBK equation with the kernel from



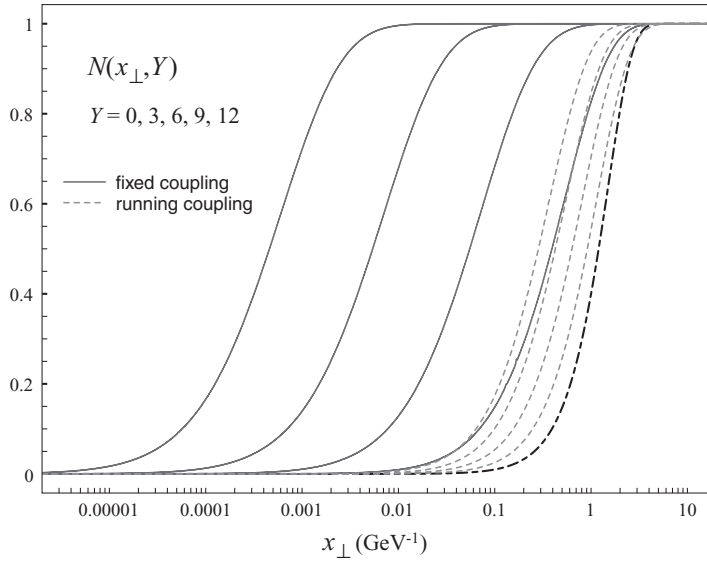


Fig. 6.3. The dipole amplitude  $N(x_{\perp}, Y)$  as a function of the dipole size  $x_{\perp}$ , plotted for several rapidities  $Y$  generated by fixed-coupling BK evolution with  $\alpha_s = 0.4$  (solid lines) and by running-coupling evolution (dashed lines) for the same initial condition (thick dashed line). (We thank Javier Albacete for providing us with this figure.) A color version of this figure is available online at [www.cambridge.org/9780521112574](http://www.cambridge.org/9780521112574).

Eq. (6.12) (and with the strong coupling “frozen” in the IR at  $\alpha_s = 1$ ) is shown in Fig. 6.3 by the dashed lines. It may be compared with the fixed-coupling BK evolution with  $\alpha_s = 0.4$  (the solid lines) for the same initial condition from Eq. (4.205). The figure depicts the dipole scattering amplitude  $N$  plotted as a function of the dipole size  $x_{\perp}$  for several different rapidities. It is clear that the fixed-coupling evolution, shown by the solid lines, is faster than the running-coupling evolution, shown by the dashed lines: the fixed-coupling curves grow faster with rapidity and the saturation scale corresponding to the fixed-coupling curves is clearly larger than that for the running coupling. Thus Fig. 6.3 illustrates property (i) in the above list.

Property (ii) is partially demonstrated in Fig. 4.32, where one can see that the two geometric scaling functions, for running and for fixed coupling, are in fact different in shape. Property (iii) is derived analytically below along with properties (i) and (ii).

Many qualitative and some quantitative features of the solution for rcBK evolution can be obtained analytically using an approximation in which a simple running of the coupling with the parent-dipole size,  $\alpha_s(x_{10}^2)$ , is used in the kernel (6.10) instead of the more complicated exact results seen in Eqs. (6.12) and (6.14). In an impact-parameter-independent approximation we can write the BK equation, by analogy with Eq. (4.175), as

$$\partial_Y \tilde{N}(\rho, Y) = \bar{\alpha}_s(\rho) \chi(-\partial_{\rho}) \tilde{N}(\rho, Y) - \bar{\alpha}_s \tilde{N}^2(\rho, Y), \tag{6.18}$$

where now

$$\rho = \ln \frac{k_{\perp}^2}{\Lambda_{QCD}^2} \tag{6.19}$$

and

$$\bar{\alpha}_s(\rho) = \frac{\alpha_s(\rho)N_c}{\pi} = \frac{N_c}{\pi\beta_2\rho} = \frac{N_c}{\pi\beta_2 \ln(k_{\perp}^2/\Lambda_{QCD}^2)}. \tag{6.20}$$

Let us analyze Eq. (6.18) using the semiclassical approximation of Sec. 4.5.3. Writing  $\tilde{N} = e^{\Omega}$  and neglecting the derivatives of  $\Omega$  of second order and higher, we rewrite Eq. (6.18) as (cf. Eq. (4.178))

$$\partial_Y \Omega = \bar{\alpha}_s(\rho)\chi(-\partial_{\rho}\Omega) - \bar{\alpha}_s e^{\Omega}. \tag{6.21}$$

Defining  $-\gamma \equiv \Omega_{\rho}$  and  $\omega \equiv \Omega_Y$  we get

$$F \equiv \omega - \bar{\alpha}_s(\rho)\chi(\gamma) + \bar{\alpha}_s(\rho)e^{\Omega} = 0. \tag{6.22}$$

The equations for the characteristics are:

$$\frac{d\rho}{dt} = F_{-\gamma} = \bar{\alpha}_s(\rho) \frac{d\chi(\gamma)}{d\gamma}, \tag{6.23a}$$

$$\frac{dY}{dt} = F_{\omega} = 1, \tag{6.23b}$$

$$\frac{d\gamma}{dt} = -F_{\rho} - (-\gamma)F_{\Omega} = \frac{d\bar{\alpha}_s(\rho)}{d\rho}\chi(\gamma) + \left[ \bar{\alpha}_s(\rho)\gamma - \frac{d\bar{\alpha}_s(\rho)}{d\rho} \right] e^{\Omega}, \tag{6.23c}$$

$$\frac{d\omega}{dt} = -F_Y - \omega F_{\Omega} = -\bar{\alpha}_s(\rho)\omega e^{\Omega}, \tag{6.23d}$$

$$\frac{d\Omega}{dt} = (-\gamma)F_{-\gamma} + \omega F_{\omega} = -\bar{\alpha}_s(\rho)\gamma \frac{d\chi(\gamma)}{d\gamma} + \omega. \tag{6.23e}$$

Again,  $Y = t$  results from Eq. (6.23b). Eliminating  $\omega$  using Eq. (6.22) and noticing that  $d\bar{\alpha}_s(\rho)/d\rho = -\bar{\alpha}_s(\rho)/\rho$  yields

$$\frac{d\rho}{dY} = \bar{\alpha}_s(\rho) \frac{d\chi(\gamma)}{d\gamma}, \tag{6.24a}$$

$$\frac{d\gamma}{dY} = -\frac{\bar{\alpha}_s(\rho)}{\rho}\chi(\gamma) + \bar{\alpha}_s(\rho) \left( \gamma + \frac{1}{\rho} \right) e^{\Omega}, \tag{6.24b}$$

$$\frac{d\Omega}{dY} = \bar{\alpha}_s(\rho) \left[ \chi(\gamma) - \gamma \frac{d\chi(\gamma)}{d\gamma} - e^{\Omega} \right]. \tag{6.24c}$$

Working in the linearized regime, we can neglect  $e^{\Omega}$  in Eq. (6.24c) and obtain the critical trajectory along which  $\Omega \approx \text{const}$ , with the critical value of the anomalous dimension  $\gamma$

specified by

$$\chi(\gamma_{cr}) = \gamma_{cr} \frac{d\chi(\gamma_{cr})}{d\gamma_{cr}}, \quad (6.25)$$

so that  $\gamma_{cr} \approx 0.6275$ , just as in the fixed-coupling case.

Solving Eq. (6.24a) along the critical (saturation) trajectory yields

$$\rho_s^2(Y) = \rho_0^2 + \frac{2N_c}{\pi\beta_2} \frac{\chi(\gamma_{cr})}{\gamma_{cr}} Y, \quad (6.26)$$

where we have imposed the initial condition

$$\rho_s(Y=0) = \ln \frac{Q_{s0}^2}{\Lambda_{QCD}^2} \equiv \rho_0. \quad (6.27)$$

Since  $\rho_s(Y) = \ln(Q_s^2(Y)/\Lambda_{QCD}^2)$ , we obtain the saturation scale in the running-coupling case (Gribov, Levin, and Ryskin 1983):

$$Q_s^2(Y) = \Lambda_{QCD}^2 \exp \left\{ \sqrt{\frac{2N_c}{\pi\beta_2} \frac{\chi(\gamma_{cr})}{\gamma_{cr}} Y + \ln^2 \frac{Q_{s0}^2}{\Lambda_{QCD}^2}} \right\}. \quad (6.28)$$

Comparing this result with the fixed-coupling saturation scale in Eq. (4.156) we see that the saturation scale in the running-coupling case grows *more slowly* with rapidity  $Y$ , confirming property (i) above stating that the running-coupling corrections slow down small- $x$  evolution. This property of the running-coupling solution is very important: as the reader may remember, the fixed-coupling BFKL intercept (6.1) is too large to describe any data. The slower growth of the running-coupling solution makes phenomenological applications of rcBK and rcJIMWLK much more successful.

Equation (6.28) has another important property: at very large rapidity we can neglect the rapidity-independent logarithm squared under the square root, since it eventually becomes small compared with the term linear in  $Y$ . This gives

$$Q_s^2(Y) \approx \Lambda_{QCD}^2 \exp \left\{ \sqrt{\frac{2N_c}{\pi\beta_2} \frac{\chi(\gamma_{cr})}{\gamma_{cr}} Y} \right\}. \quad (6.29)$$

We see that all the  $Q_{s0}$ -dependence has disappeared. Since the dependence of the saturation scale on the atomic number  $A$  comes in only through  $Q_{s0}^2 \sim A^{1/3}$ , we conclude that at very large rapidity the running-coupling saturation scale becomes independent of  $A$  (Levin and Ryskin 1987, Mueller 2003). This demonstrates property (iii) above. Therefore, at extremely high energies the parton densities in the proton and in the nucleus will be the same. While this conclusion may be somewhat disappointing, note that our analysis applies to asymptotic energies: for the energies available in modern experiments the nuclei still provide a strong enhancement of the saturation scale.

A more careful evaluation of the high energy asymptotics of the saturation scale in the running-coupling case yields

$$Q_s^2(Y) = \Lambda_{QCD}^2 \exp \left\{ \sqrt{\frac{2 N_c \chi(\gamma_{cr})}{\pi \beta_2 \gamma_{cr}}} Y + \frac{3}{4} \xi_1 \left[ \frac{N_c \chi''(\gamma_{cr})}{2\pi \beta_2 \gamma_{cr} \chi(\gamma_{cr})} Y \right]^{1/6} + \text{const} + O(Y^{-1/6}) \right\}, \tag{6.30}$$

where  $\xi_1 \approx -2.338$  is the first zero of the Airy function  $\text{Ai}(\xi)$ . The first term in the exponent of Eq. (6.30) was calculated by Gribov, Levin, and Ryskin (1983) (see also Iancu, Itakura, and McLerran (2002) and Mueller and Triantafyllopoulos (2002)), while the second term was found by Mueller and Triantafyllopoulos (2002) and by Munier and Peschanski (2004a). All the terms shown explicitly in Eq. (6.30) are universal (except for the constant): they do not depend on the initial conditions for the evolution. Several new higher-order universal terms in the expansion (6.30) were found recently by Beuf (2010).

For the constant  $\gamma = \gamma_{cr}$  to be a solution of Eq. (6.24b) we need to require that the right-hand side of this equation is zero, which gives

$$e^{\Omega_{cr}} = \frac{\chi(\gamma_{cr})}{\rho_s(Y)\gamma_{cr} + 1} \approx \frac{\chi(\gamma_{cr})}{\rho_s(Y)\gamma_{cr}}. \tag{6.31}$$

This is indeed a small quantity at high energy, when  $\rho_s(Y)$  is large, justifying the linearized approximation used in deriving the above results. Since  $\rho_s(Y) \sim \sqrt{Y}$  we see that  $e^{\Omega_{cr}}$  is a slowly varying function of  $Y$ , validating our treatment of it as a constant.

Finally, just as we did to obtain Eq. (4.187), we can expand  $\Omega$  near the saturation trajectory keeping  $Y$  fixed, to get

$$\Omega \approx \Omega_{cr} + \Omega_{\rho_s}(\rho - \rho_s) = \Omega_{cr} - \gamma_{cr}(\rho - \rho_s) \tag{6.32}$$

so that

$$\tilde{N}(\rho, Y) = e^{\Omega} \propto e^{-\gamma_{cr}(\rho - \rho_s)} = \left( \frac{Q_s^2(Y)}{k_{\perp}^2} \right)^{\gamma_{cr}}, \tag{6.33}$$

where now  $Q_s^2(Y)$  is given by Eq. (6.28). We see that the geometric scaling property of the solution persists when running-coupling corrections are included. This affirms part of the claim in property (ii) above. The anomalous dimension  $\gamma_{cr}$  obtained in the semiclassical approximation for the running-coupling coupling case is the same as for the fixed-coupling evolution: hence the dependence of  $\tilde{N}$  on  $k_{\perp}$  in Eq. (6.33) is the same as in Eq. (4.188). This appears to contradict the difference in  $k_{\perp}$ -dependence of the running- and fixed-coupling BK evolution observed in the numerical simulation in Fig. 4.32. (This discrepancy was first observed by Albacete *et al.* (2005).) We believe that the accuracy of the semiclassical approximation is insufficient to detect this difference. Presumably more precise analytical solution techniques are needed to explain the difference.

6.2.3 Nonperturbative effects and renormalons\*

Nonperturbative effects in the framework of perturbative QCD stem from the asymptotic nature of the perturbation series

$$\sum_n C_n \alpha_s^n \tag{6.34}$$

and from the fact that the coefficients  $C_n$  of this series increase as  $n!$  for large  $n$ . To date there are three known sources of this  $n!$  behavior of the perturbation-series coefficients in QCD: infrared (IR) and ultraviolet (UV) renormalons and instantons (see the review 't Hooft (1979) and the paper Mueller (1992)). A running QCD coupling generates renormalons. Since we now know how to include a running coupling in the BFKL, BK, and JIMWLK equations, we should be able to find the renormalon contribution to small- $x$  evolution and estimate the contribution of nonperturbative QCD to small- $x$  physics. Clearly the nonperturbative contribution stems from the IR renormalons, since the long distances (low momenta) corresponding to this case determine the nonperturbative corrections. Therefore we will concentrate on the IR renormalons in this section.

Since it is in line with the goal of this chapter to keep the calculations simple, let us illustrate the role of IR renormalons in saturation physics by the following toy-model example. We start with the relation between the dipole amplitude  $N$  and the unintegrated gluon distribution  $\phi$  in Eq. (6.16). Assume that it is valid in the saturation region, where one can show that  $\phi \propto k_\perp^2 / Q_s^2$ . Then the contribution of dipole amplitude in the saturation region with  $k_\perp < Q_s$  to the dipole amplitude outside the saturation region, i.e., for  $x_\perp \ll 1/Q_s$ , is proportional to

$$\int \frac{d^2 k_\perp}{k_\perp^2} \left(1 - e^{i\vec{k}_\perp \cdot \vec{x}_\perp}\right) \alpha_s(k_\perp^2) \frac{k_\perp^2}{Q_s^2}. \tag{6.35}$$

In the  $k_\perp < Q_s, x_\perp \ll 1/Q_s$  regime we have  $k_\perp x_\perp \ll 1$ , and the exponential in Eq. (6.35) can be expanded to yield after angular integration

$$\frac{x_\perp^2}{Q_s^2} \int_0^{Q_s^2} dk_\perp^2 k_\perp^2 \alpha_s(k_\perp^2), \tag{6.36}$$

where, for simplicity, we ignore overall constants.

Writing

$$\alpha_s(k_\perp^2) = \frac{\alpha_\mu}{1 + \alpha_\mu \beta_2 \ln(k_\perp^2 / \mu^2)}, \tag{6.37}$$

we substitute this into Eq. (6.36) and expand in powers of  $\alpha_\mu$ , obtaining

$$\frac{x_\perp^2}{Q_s^2} \alpha_\mu \sum_{n=0}^\infty (-\alpha_\mu \beta_2)^n \int_0^{Q_s^2} dk_\perp^2 k_\perp^2 \ln^n \frac{k_\perp^2}{\mu^2}. \tag{6.38}$$

Defining  $\zeta = \ln(\mu^2/k_\perp^2)$  we rewrite Eq. (6.38) as

$$\frac{x_\perp^2}{Q_s^2} \mu^4 \alpha_\mu \sum_{n=0}^\infty (\alpha_\mu \beta_2)^n \int_{\ln(\mu^2/Q_s^2)}^\infty d\zeta \zeta^n e^{-2\zeta}. \tag{6.39}$$

For large enough  $n$ , the integral in Eq. (6.39) is dominated by  $\zeta \approx n/2$ , so that its lower limit becomes irrelevant and can be set equal to zero. After that the  $\zeta$ -integration can be easily performed, yielding

$$\frac{x_\perp^2}{2Q_s^2} \mu^4 \alpha_\mu \sum_{n \gg 1}^\infty \left(\frac{\alpha_\mu \beta_2}{2}\right)^n n!, \tag{6.40}$$

which is a divergent perturbation series with coefficients proportional to  $n!$ . This is the effect of the IR QCD renormalons. If we define the applicability of the perturbation theory by the order  $n$  at which the  $(n + 1)$ th term in the series is comparable with the  $n$ th term, we can conclude that perturbation theory breaks down for  $n \approx n_0 = 2/(\alpha_\mu \beta_2)$ . Thus the series (6.40) but terminating at  $n = n_0$  would be perturbation theory’s best guess at the exact answer.

We can also try to evaluate the series in Eq. (6.40) using the Borel resummation procedure. Namely, we rewrite the series as

$$\frac{x_\perp^2}{2Q_s^2} \mu^4 \int_0^\infty db e^{-b/\alpha_\mu} \sum_{n \gg 1}^\infty \left(\frac{\beta_2 b}{2}\right)^n, \tag{6.41}$$

where  $b$  is a dummy integration variable. Assuming that the series starts at  $n = 0$ , we resum it to obtain

$$-\frac{2}{\beta_2} \frac{x_\perp^2}{2Q_s^2} \mu^4 \int_0^\infty db e^{-b/\alpha_\mu} \frac{1}{b - 2/\beta_2}. \tag{6.42}$$

The pole at  $b = 2/\beta_2$  is known as the IR renormalon pole in the complex- $b$  Borel plane. The  $b$ -integral in Eq. (6.42) is divergent because of this renormalon pole along the integration contour: the series is not Borel-summable. While different  $\pm i\epsilon$  regularizations of the pole can be proposed, it is not clear which such regularization would be correct. Instead the consensus in the community is that the difference between the various regularization prescriptions gives us an estimate of the uncertainty due to the renormalon singularity. Therefore, to evaluate the size of this uncertainty we simply need to take the residue of the renormalon pole, which gives

$$\sim \frac{x_\perp^2}{Q_s^2} \mu^4 e^{-2/(\alpha_\mu \beta_2)} = \frac{x_\perp^2}{Q_s^2} \Lambda_{QCD}^4. \tag{6.43}$$

The fact that the result is proportional to  $\Lambda_{QCD}^4$  indicates the nonperturbative origin of the uncertainty. The physical meaning of this phenomenon is well known (see Mueller (1985) and Zakharov (1992)). Indeed, the typical value of the momentum in the integral in

Eq. (6.38) is

$$k_{\perp}^2 \sim \mu^2 e^{-n/2} \quad (6.44)$$

and, regardless of the value of the renormalization scale  $\mu$ , at sufficiently large  $n$  this momentum will become very small, so small that we would not be able to use perturbative QCD in our calculations ( $k_{\perp} \approx \Lambda_{QCD}$ ). Of course we cannot trust our calculation for the low momenta of Eq. (6.44): instead we consider this equation as an indication that perturbation theory is breaking down and we should examine nonperturbative contributions to the observable.

The uncertainty (6.43) of our perturbative estimate should be compared with the perturbative estimate itself. If we forget the contribution of the Landau pole at  $k_{\perp} = \Lambda_{QCD}$  in Eq. (6.36) (since, effectively, we have estimated the size of that contribution in Eq. (6.43)), the rest of the integral is clearly dominated by the upper limit of integration, giving an answer proportional to

$$\sim x_{\perp}^2 Q_s^2 \alpha_s(Q_s^2). \quad (6.45)$$

Comparing Eq. (6.43) with Eq. (6.45) we see that the relative contribution of the nonperturbative IR renormalon corrections is of order

$$\frac{\Lambda_{QCD}^4}{Q_s^4} \ll 1. \quad (6.46)$$

We conclude that saturation effects tend to suppress the renormalon contribution. Equation (6.46) is analogous to the conclusion by Mueller (1985) and Zakharov (1992) that the renormalon contribution in  $e^+e^-$  annihilation is of order  $\Lambda_{QCD}^4/Q^4$ , i.e., it is a higher-twist effect. In our case IR renormalons are also higher twist and, importantly, they are not enhanced by powers of  $A^{1/3}$  or powers of  $1/x$  and are therefore subleading compared with the perturbative saturation effects.

The qualitative conclusions of our toy model presented above are substantiated by more detailed calculations. The interested reader is referred to the papers by Levin (1995) and by Gardi *et al.* (2007) for much more detailed analytical and numerical investigations on the subject.

### 6.3 The next-to-leading order BFKL and BK equations

The NLO (order- $\alpha_s^2$ ) corrections to the kernels of the BFKL and BK equations are now known. The NLO BFKL kernel was found by Fadin and Lipatov (1998) and Ciafaloni and Camici (1998), while the NLO BK equation was constructed by Balitsky and Chirilli (2008). Here we will briefly outline the calculational strategy and the main physical conclusions stemming from these calculations.

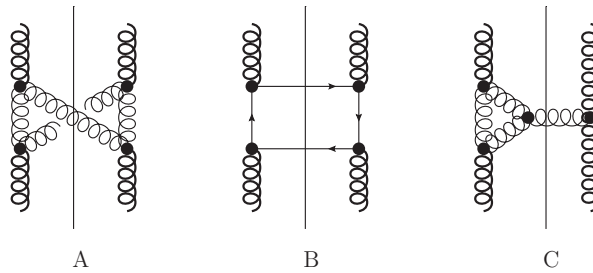


Fig. 6.4. Examples of diagrams contributing next-to-leading order corrections to the BFKL kernel. The bold lines denote reggeized gluons, and the circles denote regular QCD vertices. The vertical solid straight lines represent cuts.

### 6.3.1 Short summary of NLO calculations

It took almost a decade from the first papers on the subject (Fadin and Lipatov 1989, Ciafaloni 1988) to the last (Fadin and Lipatov 1998, Ciafaloni and Camici 1998) to solve the problem of finding the NLO BFKL kernel. As discussed above, the LO BFKL is a sum of ladder diagrams with Lipatov effective vertices and with reggeized gluons in the  $t$ -channel. The NLO corrections to this ladder include the running-coupling corrections to the vertices in the ladder (see for example Fig. 6.4C) and also processes involving the emission of two gluons with comparable rapidities in a single rung (see Fig. 6.4A). One also needs to calculate the quark–antiquark pair production (see Fig. 6.4B) and to find the reggeized gluon trajectory in the NLO approximation. (Of course one also has to prove that we can still use the reggeized gluon in the NLO approximation: this turns out to be the case.) The relative simplicity of the LO BFKL equation originates in part from the fact that in the LLA one can easily separate the longitudinal and transverse degrees of freedom. In the NLO approximation one has to take into account the fact that the limits of integration over longitudinal momenta depend also on the transverse momenta. The large number of extra diagrams, a tiny subset of which is shown in Fig. 6.4, along with the more sophisticated diagram evaluation required in a beyond-LLA approximation, are the two main reasons why it took so long to find the NLO BFKL kernel.

The exact NLO BFKL kernel is too cumbersome to be presented here. It can be found in the papers of Fadin and Lipatov (1998) and Ciafaloni and Camici (1998). The results of these calculations yielded some new features and new questions. The NLO corrections to the LO BFKL intercept turned out to be negative. Such negative corrections had been expected, since the LO BFKL intercept given in Eq. (6.1) is too large: this is why the LO BFKL evolution overestimates the rise of the DIS structure functions with energy as well as the size of the Bjorken scaling violation  $dF_2/d \ln Q^2$  in comparison with the HERA experimental data. However, the size of the negative NLO corrections turned out to be too large. The BFKL pomeron intercept in the saddle point approximation for the LO and NLO orders is equal to (cf. the LO BFKL intercept in Eq. (3.86))

$$\alpha_P - 1 \approx 4 \bar{\alpha}_s \ln 2 (1 - 6.7 \bar{\alpha}_s). \quad (6.47)$$



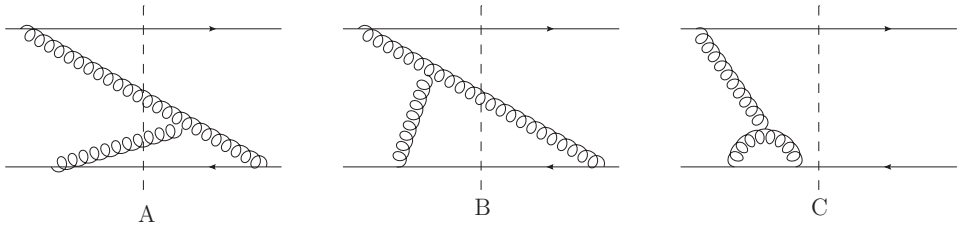


Fig. 6.5. Examples of diagrams contributing NLO corrections to the BK and JIMWLK kernels.

Equation (6.47) leads to a negative intercept for  $\bar{\alpha}_s > 1/6.7 \approx 0.15$ , which means that the NLO BFKL pomeron leads to structure functions that fall off with energy at all virtualities up to  $Q^2 \approx 10^3 \text{ GeV}^2$ . This result points toward an instability of the NLO BFKL pomeron, and this is confirmed by the oscillatory behavior of the resulting NLO gluon density. (The reader is also referred to Ross (1998), where it is shown that, in the cross section mediated by NLO BFKL pomeron exchange in the diffusion approximation, the logarithm squared term in the exponent (see Eq. (3.85)) enters with a plus sign, indicating an instability of the solution due to the enhancement of transverse momentum fluctuations.)

The NLO BFKL kernel appears to lead to a number of serious questions, which may be resolved by the calculation of the higher-order corrections. Unfortunately, owing to the apparent complexity of the NNLO calculations, it looks unreasonable to expect the result soon. Fortunately, it turns out that the most numerically essential contribution in the NLO BFKL kernel comes from collinear singularities, which are resummed by the DGLAP evolution. The resummation of collinear corrections to the BFKL kernel appears to cure the instability of the NLO BFKL pomeron, as we will discuss in the next section.

It is also possible that some problems of NLO BFKL would be cured by a consideration of saturation effects. To check this, one has to study the nonlinear BK and JIMWLK evolution equations at NLO. The NLO BK equation was calculated by Balitsky and Chirilli (2008) (see also Balitsky and Belitsky (2002) for a calculation of part of the kernel). A small subset of the diagrams that one has to calculate in order to find the NLO BK kernel is shown in Fig. 6.5. In one step of NLO evolution one has to emit two  $s$ -channel gluons with comparable rapidities. The diagrams can be classified by the number of gluons interacting with the target: there may be zero, one, or two gluons, as shown in Figs. 6.5C, B, A respectively. Indeed, one should also include one-loop quark corrections, illustrated by the lowest-order (one-loop) case of the diagrams in Fig. 6.1. Note that, in the large- $N_c$  limit, diagrams of the type shown in Fig. 6.5A imply that the parent dipole will split into *three* daughter dipoles, resulting in an evolution equation which is cubic in  $N$  (or  $S$ ) (Balitsky and Belitsky 2002). Hence the quadratic structure of the LO BK evolution does not survive at higher orders.

As in the BFKL case, the calculation of the NLO BK evolution is too technically involved to be presented here; we refer the reader to the paper by Balitsky and Chirilli (2008) for details. In the linearized limit, the NLO BK evolution indeed reduces to the NLO BFKL evolution. Unfortunately, at this time the physical implications of NLO BK evolution are not completely understood.

### 6.3.2 Renormalization-group-improved NLO approach\*

Let us now present a strategy to cure the problems of the NLO BFKL kernel by performing the resummation of collinear singularities to all orders. This procedure was suggested in the works of Salam (1998, 1999) and Ciafaloni, Colferai, and Salam (1999a). The key idea is based on the observation that the large NLO corrections to the BFKL kernel stem mostly from collinearly enhanced physical contributions. At the same time we know that the collinear singularities can be resummed with the help of the renormalization group (RG) and have been taken into account in the DGLAP evolution. The idea of finding a combined description that includes the BFKL anomalous dimension with the anomalous dimension of the DGLAP evolution equation has a history ranging from the first attempt by Gribov, Levin, and Ryskin, where the DGLAP anomalous dimension was simply added to the BFKL anomalous dimension, to the Catani, Ciafaloni, Fiorani and Marchesini (CCFM) evolution equation, in which a correct treatment of the coherence effect in the collinear kinematics was introduced. In the renormalization-group-improved NLO approach this problem was solved, and we will follow the paper of Ciafaloni, Colferai, and Salam (1999a) in our discussion of the theoretical approach. We will also present the next-to-leading-order resummed BFKL kernel in the simple form given in the paper of Khoze *et al.* (2004) to illustrate the numerical importance of the corrections that were introduced.

The starting point is the expression for the azimuthally symmetric Green function of the BFKL pomeron in the double Mellin representation, namely (cf. Eqs. (3.78) and (3.80) with  $n = 0$ )

$$G(k, k_0, Y) = \frac{1}{k^2} \int_{a-i\infty}^{a+i\infty} \frac{d\omega}{2\pi i} \int_{1/2-i\infty}^{1/2+i\infty} \frac{d\gamma}{2\pi^2 i} \left(\frac{s}{kk_0}\right)^\omega e^{\gamma\xi} \frac{1}{\omega - \kappa(\gamma, \omega)}, \quad (6.48)$$

where  $k$  and  $k_0$  with  $k > k_0$  are the transverse momentum scales at the ends of the ladder, with  $\xi = \ln(k^2/k_0^2)$ , and the integration contour over  $\omega$  in Eq. (6.48) lies to the right of all the singularities of the integrand. We have also replaced the rapidity  $Y$  by  $\ln(s/(kk_0))$ . For the LO BFKL the function  $\kappa(\gamma, \omega)$  reduces to  $\kappa_{LO}(\gamma, \omega) = \bar{\alpha}_s \chi(\gamma)$ , with the latter given by Eq. (4.174). In the LO case, integrating over  $\omega$  in Eq. (6.48) yields Eq. (3.80) with  $n = 0$ .

It is clear from Eq. (6.48) that the traditional DGLAP moment-space representation (see Sec. 2.4.5) can be achieved after the integration over  $\gamma$  by closing the contour to pick up the singularity at  $\gamma = \gamma(\bar{\alpha}_s, \omega)$ , which is the solution of the equation

$$\omega = \kappa(\gamma, \omega). \quad (6.49)$$

The result of the calculation of the NLO BFKL equation allows one to write

$$\kappa(\gamma, \omega) = \bar{\alpha}_s \chi(\gamma) + \bar{\alpha}_s^2 \chi_1(\gamma, \omega) + \dots, \quad (6.50)$$

where the exact form of the NLO correction  $\chi_1(\gamma, \omega)$  is unimportant for our purposes. We only need to know that an inspection of the explicit form of  $\chi_1(\gamma, \omega)$  shows that numerically large contributions stem from the regions  $\gamma \rightarrow 0$  and  $\gamma \rightarrow 1$ , where  $\chi_1(\gamma, \omega) \propto 1/\gamma^2$  and

$1/(1 - \gamma)^2$  respectively. These are the regions of  $\gamma$  where the DGLAP equation governs the energy and transverse momentum evolution of the parton densities, which will be utilized shortly.

Another large contribution originates from the dependence of the QCD coupling on the transverse momenta. This contribution can be incorporated in the framework of the RG approach if we first integrate over  $\gamma$  in Eq. (6.48); then, solving Eq. (6.49) to find the pole at  $\gamma(\bar{\alpha}_s, \omega)$  and, for  $k > k_0$ , making the replacement

$$\gamma(\bar{\alpha}_s(\xi), \omega) \xi \longrightarrow \int_0^\xi d\xi' \gamma(\bar{\alpha}_s(\xi'), \omega) \tag{6.51}$$

in the exponent of Eq. (6.48) would give us the answer as a single integral over  $\omega$  with the running-coupling corrections included.

Our aim is to find a function  $\kappa(\gamma, \omega)$  that describes both the LO and NLO BFKL kernels and DGLAP evolution for  $k^2 > k_0^2$  (or  $k_0^2 > k^2$ ). A comparison of Eq. (6.48) with the DGLAP equation shows that since the latter is written in terms of the distribution functions, the definition of Bjorken  $x$  (and consequently of the rapidity  $Y = \ln 1/x$ ) in the DGLAP picture is given by  $x = k^2/s$  for  $k^2 \gg k_0^2$  and by  $x = k_0^2/s$  for  $k^2 \ll k_0^2$ ; these expressions are different from those for an up-down symmetric (for a vertically drawn ladder) variable  $x = e^{-Y} = (k_0 k)/s$  used in Eq. (6.48). Indeed, in the LLA small- $x$  evolution such differences were outside the approximation’s control and were not important: now they are crucial for matching NLO BFKL onto DGLAP evolution. Changing the momentum scale in the definition of rapidity and Bjorken  $x$  leads to the shift  $\gamma \rightarrow \gamma \pm \omega/2$ :

$$\begin{aligned} G(k, k_0, Y) &= \frac{1}{k^2} \int_{a-i\infty}^{a+i\infty} \frac{d\omega}{2\pi i} \int_{1/2-i\infty}^{1/2+i\infty} \frac{d\gamma}{2\pi^2 i} \left(\frac{s}{k^2}\right)^\omega e^{(\gamma+\omega/2)\xi} \frac{1}{\omega - \kappa(\gamma, \omega)} \\ &= \frac{1}{k_0^2} \int_{a-i\infty}^{a+i\infty} \frac{d\omega}{2\pi i} \int_{1/2-i\infty}^{1/2+i\infty} \frac{d\gamma}{2\pi^2 i} \left(\frac{s}{k_0^2}\right)^\omega e^{(1-\gamma+\omega/2)\xi_0} \frac{1}{\omega - \kappa(\gamma, \omega)}, \end{aligned} \tag{6.52}$$

where we have defined  $\xi_0 = \ln(k_0^2/k^2)$  to replace  $\xi$  in the case  $k_0 > k$ . We see that one effect of DGLAP evolution would be to replace  $\gamma$  by  $\gamma + \omega/2$  near the singularity  $\gamma = 0$  and  $\gamma$  by  $\gamma - \omega/2$  near the singularity  $\gamma = 1$ .

The LO BFKL kernel has singularities for all integer values of  $\gamma$ , corresponding to different powers of  $k^2/k_0^2$  in the Green function  $G$ , that is, to different twists. Singling out the leading-twist singularities at  $\gamma = 0$  and  $\gamma = 1$  we write the LO BFKL kernel as a sum of the leading-twist contribution and the higher-twist terms:

$$\chi(\gamma) = \frac{1}{\gamma} + \frac{1}{1 - \gamma} + \chi^{HT}(\gamma) \tag{6.53}$$

where the higher-twist part is given by

$$\chi^{HT}(\gamma) = 2\psi(1) - \psi(1 + \gamma) - \psi(2 - \gamma). \tag{6.54}$$

The two terms of the leading-twist part of  $\chi(\gamma)$  describe two different branches of the leading-twist evolution: the  $1/\gamma$  term corresponds to a DGLAP evolution from low  $k_0$  to high  $k$  with ordering in the transverse momenta of emitted partons  $k_0 \ll k_{1\perp} \ll \dots \ll k_{i\perp} \ll \dots \ll k$ , while the  $1/(1-\gamma)$  term leads to an evolution from low  $k$  to high  $k_0$  with the opposite ordering,  $k \ll \dots \ll k_{i\perp} \ll \dots \ll k_{1\perp} \ll k_0$ . The higher-twist contributions play a significant role in the LO BFKL evolution: for example, they change the leading-twist value of the pomeron intercept from  $[1/\gamma + 1/(1-\gamma)]_{\gamma=1/2} = 4$  to  $\chi(\gamma = 1/2) = 4 \ln 2 \approx 2.8$ . However, the DGLAP evolution or, in other words, the anomalous dimensions of the operators giving rise to the higher-twist contributions are entirely unknown. Fortunately, on scrutinizing the NLO BFKL kernel one can see that the large problematic contribution does not come from these higher-twist terms and so we can concentrate on the leading-twist terms alone.

The next step is to replace the residue 1 in the first term in Eq. (6.53) by the full DGLAP gluon–gluon anomalous dimension  $\gamma_{GG}(\omega)$  from Eq. (2.121d), in order to incorporate the DGLAP effects at finite  $\omega$ :

$$\frac{\bar{\alpha}_s}{\gamma} \rightarrow \frac{\bar{\alpha}_s}{2N_c} \frac{\omega \gamma_{GG}(\omega)}{\gamma}. \quad (6.55)$$

Performing the same replacement for the term  $1/(1-\gamma)$  in Eq. (6.53) and using the shifts in  $\gamma$  incorporated into Eq. (6.52), we obtain the RG-improved BFKL kernel (Ciafaloni, Colferai, and Salam 1999a):

$$\kappa_{RG}(\gamma, \omega) = \frac{\bar{\alpha}_s}{2N_c} \left[ \frac{\omega \gamma_{GG}(\omega)}{\gamma + \omega/2} + \frac{\omega \gamma_{GG}(\omega)}{1 - \gamma + \omega/2} \right] + \bar{\alpha}_s \chi^{HT}(\gamma) + \dots, \quad (6.56)$$

where the ellipsis stand for order- $\alpha_s^2$  terms that are nonsingular at  $\gamma = 0$  and  $\gamma = 1$ . The expansion of Eq. (6.56) in powers of  $\omega$  would give us the correct collinear singularities ( $1/\gamma^2$  and  $1/(1-\gamma)^2$  terms) at the NLO at order  $\omega$ , while higher orders in  $\omega$  capture the collinear singularities of the higher-order BFKL kernels.

The kernel in Eq. (6.56) contains the full LO and NLO BFKL kernels, with the leading-twist parts of the LO BFKL kernel enhanced by DGLAP evolution, which resums all the leading (transverse) logarithmic collinear singularities to all orders.

To impose energy conservation one has to make sure that the kernel (6.56) vanishes at  $\omega = 1$  (see Exercise 2.3). This can be achieved in a crude way by simply multiplying  $\chi^{HT}(\gamma)$  and other terms in Eq. (6.56) that are *a priori* nonvanishing at  $\omega = 1$  by  $1 - \omega$  (Ellis, Kunszt, and Levin 1994). The expression that results from this procedure, after the terms denoted by the ellipsis in Eq. (6.56) have been discarded,

$$\kappa_{RG}(\gamma, \omega) = \frac{\bar{\alpha}_s}{2N_c} \left[ \frac{\omega \gamma_{GG}(\omega)}{\gamma + \omega/2} + \frac{\omega \gamma_{GG}(\omega)}{1 - \gamma + \omega/2} \right] + (1 - \omega) \bar{\alpha}_s \chi^{HT}(\gamma), \quad (6.57)$$

was used by Khoze *et al.* (2004), who showed that Eq. (6.57) describes the full RG-resummed NLO BFKL kernel (6.56) within 7% accuracy. The most interesting aspect of the result is that even such a simple modification of the NLO BFKL kernel leads to a stable result for the Green function, and for the resulting amplitudes and cross sections, and considerably reduces the value of the NLO corrections. The kernel (6.56) has a minimum at  $\gamma = 1/2$ , at

which the value of the BFKL pomeron intercept is about 0.25 for  $\bar{\alpha}_s = 0.15$ . The diffusion logarithm squared term (similar to Eq. (3.85)) again has a negative coefficient, so that the instability of transverse momentum fluctuations is now avoided. In the region  $\gamma < 1/2$  the NLO kernel (6.57) is very close to the DGLAP kernel. For a detailed comparison of the modified BFKL kernel with the experimental data as well as with other approaches we recommend the paper Ciafaloni (2005).

We have demonstrated that our knowledge of DGLAP evolution allows us to understand the sources of the large NLO contributions to the BFKL equation and allows us to formulate a more stable approach to higher-order corrections for small- $x$  evolution.

The effect of the NLO corrections on the value of the saturation scale was considered by Gotsman *et al.* (2005); not unexpectedly, their conclusion was that the NLO corrections, while lowering the value of the BFKL intercept, also slow down the growth in the saturation scale with energy, leading to lower values of the saturation scale than those given by the fixed-coupling evolution.

### Further reading

The first attempts to include the running QCD coupling in the BFKL equation by resumming powers of  $\alpha_s N_f$  were made by Braun (1995) and Levin (1995) and were based on the bootstrap equation (see Sec. 3.3.5) at next-to-leading order, obtaining the triumvirate of running couplings for the first time. Their original conjecture was proved at NLO by Fadin and Fiore (1998). The direct calculations in the BK/JIMWLK formalism discussed above were performed by Balitsky (2007) and by Kovchegov and Weigert (2007a).

For more information on the nonperturbative corrections to BFKL, BK, and JIMWLK evolution coming from the IR renormalons, we refer the reader to Gardi *et al.* (2007) and Levin (1995). Some aspects of the nonperturbative effects due to instantons in the CGC were studied by Kharzeev, Kovchegov, and Levin (2002). The possibility that the BFKL pomeron could reach the nonperturbative region of small momenta through “tunneling” was suggested by Ciafaloni *et al.* (2003b). Whether the nonlinear evolution can withstand this type of nonperturbative correction and remain perturbative is still an open question.

The NLO BFKL kernel has been calculated by two groups: Fadin, Lipatov, and their collaborators and Camici, Ciafaloni, and their collaborators. All references for these works can be found in the papers with the final results: Fadin and Lipatov (1998) and Ciafaloni and Camici (1998). The NLO BK equation was found by Balitsky and Chirilli (2008).

In our presentation of the RG-improved BFKL kernel we described the key ideas proposed by Salam (1998, 1999) and by Ciafaloni, Colferai, and Salam (1999a). We discussed the simplest possible example of a resummed kernel, that from the paper of Khoze *et al.* (2004). More recent developments in this area can be found in the papers by Ciafaloni *et al.* (2003a) and by Altarelli, Ball, and Forte (2006). We need to remember that we have no information on the anomalous dimensions of the higher-twist contributions and, therefore, the NLO corrections to the part of the BFKL kernel that is responsible for the higher-twist corrections cannot be improved on the basis of the existing renormalization group. This problem is not for further reading but rather for further research. Alternatives to the

RG-improved BFKL kernel can be found in the papers by Brodsky *et al.* (1999) and by Schmidt (1999). For a description of the experimental DIS data in the NLO BFKL approximation we refer the reader to the papers White and Thorne (2007), Ciafaloni (2005), and Peschanski, Royon, and Schoeffel (2005). The effect of the NLO BFKL kernel on the saturation scale was studied by Khoze *et al.* (2004). The impact of NLO corrections on the solution of the BK equation was studied by Gotsman *et al.* (2004). The large contribution of the NLO correction to the saturation scale possibly calls for a generalization of the nonlinear equation and could be a good subject for further investigations.

### Exercises

**6.1** Using Eq. (6.56) (dropping the ellipses) with the gluon–gluon splitting function  $\gamma_{GG}$  given by Eq. (2.121d), calculate the correction to the intercept of the BFKL pomeron, as follows.

(a) Solve

$$\omega = \kappa_{RG}(\gamma, \omega) \quad (6.58)$$

for  $\omega$  by assuming that  $\omega = O(\bar{\alpha}_s)$  and expanding the right-hand side to the quadratic order in  $\omega$ .

(b) Find the saddle point of the resulting expression for  $\omega(\gamma)$ ; the value of  $\omega(\gamma)$  at the saddle point yields the new BFKL pomeron intercept.

(c) Find the Green function (6.48) in the diffusion approximation using the results of parts (a) and (b). Show that the diffusion term is negative and, therefore, the solution is stable.

**6.2** Consider the analogue of the series from Eq. (6.40) in QED:

$$\sum_{n=0}^{\infty} \left( -\frac{\alpha_{EM}}{6\pi} \right)^n n!. \quad (6.59)$$

Resum the series using the Borel resummation procedure outlined in Sec. 6.2.3. Comment on the analyticity of the function of  $\alpha_{EM}$  that is obtained.